Optimal Control of a Mechanical Hybrid Powertrain

Koos van Berkel, *Student Member, IEEE*, Theo Hofman, Bas Vroemen, and Maarten Steinbuch, *Senior Member, IEEE*

***Abstract*—This paper presents the design of an optimal energy management strategy (EMS) for a low-cost mechanical hybrid powertrain. It uses mechanical components only—a flywheel, clutches, gears, and a continuously variable transmission—for its hybrid functionalities of brake energy recuperation, reduction of inefficient part-load operation of the engine, and engine shutoff during vehicle standstill. This powertrain has mechanical characteristics, such as a relatively small energy storage capacity in the form of the compact flywheel and multiple driving modes to operate the powertrain because of the use of clutches. The optimization problem is complex because it is twofold: 1) to find the optimal sequence of driving modes and 2) to find the optimal power distribution between the engine, the flywheel, and the vehicle. Dynamic programming is used to compute the globally optimal EMS for six representative driving cycles. The main design criterion is the minimization of the overall fuel consumption, subject to the system's kinematics, dynamics, and constraints. The results provide a benchmark of the fuel-saving potential of this powertrain design and give insight into the optimal utilization of the flywheel system. In addition, the complexity (and computation time) of the problem is reduced by *a priori* (static) optimization of the power distribution for each driving mode. Static optimization of a dynamic optimization problem yields a suboptimal solution; however, the results show that the consequences on the fuel saving are small with respect to the optimal one (the difference is $< 0.8\%$).**

***Index Terms*—Continuously variable transmission (CVT), energy management, flywheel, mechanical energy storage, optimal control.**

I. Introduction

HYBRID vehicles are a promising solution to the problem of reducing the fuel consumption and carbon dioxide emission for passenger vehicles. Hybridization of a powertrain implies adding a secondary power source to a primary power source (engine) to improve its functionality and performance. The hybrid component is a bidirectional power source able to store and exchange energy with the primary power source and the driven (vehicle) load. Currently, state-of-the-art hybrid electric vehicles (HEVs) offer fuel savings typically ranging from 5% to 30%, depending on the degree of hybridization, the reference vehicle, driving cycle, and energy management strategy (EMS), among others. However, the additional cost of most hybrid powertrains, as compared with their conventional counterparts, is relatively high due to costly electrical components such as large battery packs, high-power electronic power converters, and additional motor(s) and/or generator(s). In addition to costs, batteries also suffer from technical drawbacks, such as a low specific power, a limited efficiency, and a limited lifetime [1]. For the emerging vehicle market, e.g., China, hybridization of vehicles is of great interest due to the increasing oil price and stricter environmental legislation. However, such high additional costs may not be acceptable in this cost-sensitive market.

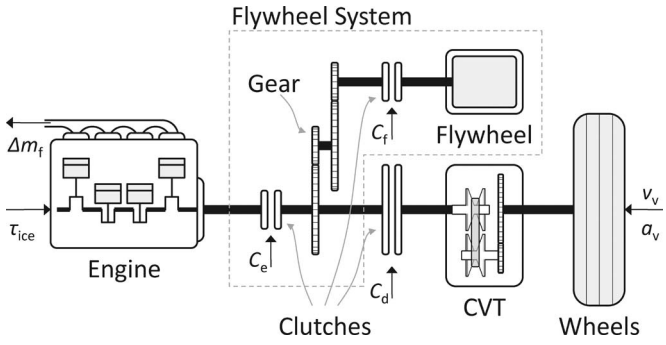

Fig. 1. Hybrid powertrain topology and signal flow, including the ICE, FS, clutches, gears, and CVT.

A viable low-cost alternative is a mechanical hybrid powertrain using a flywheel and a variable speed drive for energy storage and power transmission, respectively [2]. Mechanical components are suitable to transmit high power [3] and usually have a much lower cost than equivalent high-power electric components, e.g., a factor of 10 lower for the system described by van Druten [4]. Moreover, in case the flywheel is mechanically coupled to the powertrain, no energy conversion takes place, and power can be efficiently transmitted. This paper considers the *mecHybrid* powertrain [5], which uses a compact flywheel system (FS) and a push-belt continuously variable transmission (CVT), as schematically depicted in Fig. 1. More information on this concept and its benefits compared with other (flywheel-based) mechanical hybrid powertrains can be found in [6]. This powertrain uses the CVT for smooth and fast "charging" and "discharging" of the flywheel, e.g., to recuperate brake energy and propel the vehicle, respectively. The main fuel-saving benefit can be attributed to the added hybrid functionalities:

1) brake energy recuperation (BER) for later use;
2) reduction of inefficient part-load operation of the engine, e.g., by driving purely on the flywheel with the engine shutoff or by charging the flywheel while propelling the vehicle, at fuel-efficient operation points of

Manuscript received May 24, 2011; revised August 30, 2011; accepted November 29, 2011. Date of publication December 13, 2011; date of current version February 21, 2012. The *mecHybrid* project is supported by the "Pieken in de Delta" program, which is funded by the Dutch Ministry of Economic Affairs, Province Noord-Brabant, and Samenwerkingsverband Regio Eindhoven. The review of this paper was coordinated by Dr. D. Cao.

K. van Berkel, T. Hofman, and M. Steinbuch are with the Department of Mechanical Engineering, Eindhoven University of Technology, 5600 MB Eindhoven, The Netherlands (e-mail: k.v.berkel@tue.nl).

B. Vroemen is with Drivetrain Innovations B.V. (DTI), 5653 LD Eindhoven, The Netherlands.

Color versions of one or more of the figures in this paper are available online at http://ieeexplore.ieee.org.

Digital Object Identifier 10.1109/TVT.2011.2178869

the engine—this functionality is, however, limited by the relatively small energy storage capacity of the flywheel;
3) engine shutoff during vehicle standstill (or idle-stop).

This paper will not consider the design issues related to sizing and choice of components but will focus on the EMS designs for such hybrids.

A. EMS

To make full use of the hybrid functionalities, an EMS is required that manages the power flows at the system level by creating set points for the low-level component controllers that control the dynamics in the hybrid powertrain. The main question follows [7]: *How can the secondary mover, i.e., the FS, be utilized to minimize the fuel consumption without compromising comfort issues, such as unexpected noise produced by the engine?* EMS designs may be classified into heuristic, optimal, and suboptimal controllers [8]. Strategies that are based on heuristics can be very suitable for online implementation by using a rule-based strategy or fuzzy logics [9], although it is not clear whether the result is close to the optimal solution in all situations. Optimal strategies use global optimization techniques, such as (classical) optimal control theory [10], (mixed-integer) linear programming, (sequential) quadratic programming, and dynamic programming (DP) [11]. In general, these optimal techniques do not offer an online implementable (or causal) solution because they assume that the future driving profile is exactly known. Nevertheless, their results can be used as a benchmark for the performance of other strategies or for the design of suboptimal causal strategies [12], which combine the benefits of both optimal and causal controllers—see, e.g., the equivalent consumption minimization strategy [13] or other similar methods [14]–[16].

The EMS design approach for mechanical hybrid vehicles (MHVs) may differ from that of HEVs because of different (mechanical) characteristics:

1) multiple combinations of clutch states to operate the powertrain (or driving modes) and discrete switches in between;
2) power dissipation in clutches;
3) relatively small energy storage capacity of the flywheel;
4) relatively many kinematic constraints imposed by mechanical connections.

For the considered MHV, this has consequences on the modeling of the powertrain and the complexity of the optimization problem. The design of an optimal EMS requires additional modeling details.

1) The powertrain model is hybrid, i.e., the combination of clutch states to operate the powertrain (driving mode) is described by a discrete state, whereas the powertrain dynamics are described by continuous states.
2) The power losses that result from slipping clutches cannot be neglected because of the following: 1) there are relatively frequent switches between driving modes due to the small energy storage capacity of the flywheel and the relatively many kinematic constraints; and 2) the drive clutch is used to launch the vehicle, instead of an electric machine (which usually does not require a clutch).

In addition, the optimization problem is more complex.

1) Two optimization problems are combined: 1) The *driving-mode switching* problem is to find the optimal driving modes, and 2) the *power-split* problem is to find the optimal power distribution among the main components, i.e., the engine, flywheel, and vehicle.
2) There are comfort-related constraints, e.g., to avoid high-frequent switching between driving modes while driving at constant velocity—this high-frequent switching produces an alternating engine noise that is unexpected when driving at constant velocity.

EMS design approaches for HEVs are well covered in the literature, e.g., [17] gives an overview. For MHVs, however, only a few EMS design approaches are found, which are often either heuristic [18], [19] or only optimize the power-split problem for one specific driving mode [20] without considering the driving-mode switching problem. The EMS designs described in [3] and [21] do not consider comfort-related constraints, e.g., the engine is sometimes used to charge the flywheel with full power during the standstill of the vehicle; the engine noise is expected to be unacceptable for the comfort of the driver.

B. Contribution and Outline of This Paper

This paper presents the design of an optimal EMS for the considered MHV with the previously described mechanical characteristics. DP is applied to find the optimal sequence of the control inputs (driving modes and the power split) over six representative driving cycles. The main design criterion is the minimization of the overall fuel consumption over a predefined driving cycle, subject to the system's kinematics, dynamics, and (comfort-related) constraints. The hybrid powertrain model, on which the optimal EMS is based, includes submodels that describe power losses related to engine cranking and slipping clutches. The optimization problem includes both power-split and driving-mode switching problems, which can be seen as similar to the gear-shifting problem, e.g., as described in [22] and [23]. In addition, comfort-related constraints are introduced to avoid specific driving-mode operations and switches. The additional modeling details and constraints, however, require more states to describe the system's kinematics and dynamics. Consequently, the complexity of the optimization problem increases, and with it, the computation time required to solve it also increases.

One way to reduce the number of states and control inputs is by static *a priori* optimization of the power split for each driving mode, i.e., without knowledge of the driving cycle, whereas the driving-mode switching problem is still dynamically optimized. This paper shows that, for the considered hybrid powertrain, with a statically optimized power split, the achieved fuel saving is only slightly smaller than that with the dynamically optimized power split. The results on fuel consumption provide a benchmark for the fuel-saving potential of this hybrid powertrain. Furthermore, insights are gained in the effectiveness of the hybrid functionalities, the effect of the FS on the transmission losses, and the optimal utilization of the FS.

TABLE I
BASE COMPONENT CHARACTERISTICS

Engine[1]	4-cylinder 1.5-l gasoline internal combustion engine, max. power 76 kW (at 6000 rpm), max. torque 140 Nm (at 4000 rpm), peak efficiency 230 g/kWh, drag torque 12-17 Nm.
Flywheel[1]	Vacuum-placed 150-kJ steel flywheel, power range −25-35 kW, max. speed 30 000 rpm, inertia 0.03 kgm^2, gear ratio 1:12, max efficiency 98 %, total system mass 27 kg, drag torque 0.07-0.11 Nm.
Transmission[1]	Push-belt driven Continuously Variable Transmission, torque range −100-140 Nm, ratio range 0.4-2.3, final drive ratio 1:5.41, integrated pump, max. efficiency 91 %.
Vehicle[2] + 2 passengers	Smart ForFour (2005), mass 970+150 kg, combined inertia of the wheels 1.2 kgm^2, aerodynamic drag coefficient 0.31, frontal area 1.86 m^2, static rolling resistance 143 N.

[1]Data based on experimental results. [2]Data based on estimated parameters.

The outline of this paper is given as follows: Section II describes the modeling of the components of this hybrid powertrain. Section III describes the powertrain model for different driving modes and the switches in between and introduces comfort-related constraints on both the driving modes and switches in between. Section IV defines the optimization problem and introduces two reduced optimization problems that are solved with DP. Section V presents the simulation results and analyzes the optimal EMS designs and their results. Finally, conclusions are drawn in Section VI.

II. COMPONENT MODELS

The main components of the hybrid powertrain are the internal combustion engine (ICE), FS, clutches, CVT, and vehicle. This section describes the modeling of these components, for which some characteristics are summarized in Table I. The hybrid powertrain model describes the longitudinal dynamics and is *backward facing*, i.e., the components are (implicitly) a function of the velocity and acceleration of the vehicle. Kinematics, dynamics, and constraints are modeled in a discrete-time format using a simple forward Euler scheme, with a fixed discrete-time step of $\Delta t = 1$ s. The discrete time is indicated by subscript k. Dynamic effects acting on a smaller time scale (i.e., < 1 s) are assumed to be controlled by the low-level component controllers and are, hence, not considered. For the sake of simplicity, only the most relevant (largest) inertias are considered: the inertias of the flywheel, engine, and the vehicle. Smaller inertias, such as that of clutches, gears, and the pulleys of the CVT, are expected to have a negligible effect on the fuel consumption and are hence not considered. Gear ratios are defined as the output speed (vehicle side) divided by the input speed (FS side). Some (efficiency) models are, because of their nonlinear behavior, described by lookup tables, based on static experiments performed under warm operating conditions. For such models, intermediate points are calculated by linear interpolation. The flywheel clutch is only used to synchronize the flywheel gear with the flywheel; as the inertia of this gear is not considered, this clutch does not dissipate any power and may be also modeled after the gear. The resulting dynamic model of the hybrid powertrain is shown in Fig. 2.

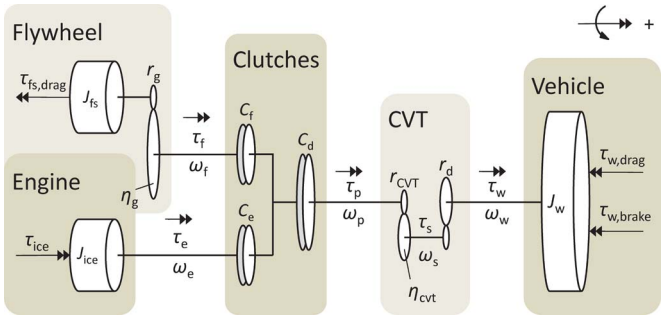

Fig. 2. Dynamic model of the hybrid powertrain (compliances are omitted).

A. ICE

The ICE is modeled by an inertia J_{ice} on which two torques are acting: the generated net torque τ_{ice}, which already includes the drag torque, and the torque on the output shaft τ_e, which depends on the selected driving mode, as will be described in Section III-A. The dynamics and constraints are given by

$$\omega_{e,k+1} = \omega_{e,k} + \frac{1}{J_{\text{ice}}}(\tau_{\text{ice},k} - \tau_{e,k})\Delta t \tag{1}$$

$$-\tau_{\text{ice,drag}}(\omega_{e,k}) \le \tau_{\text{ice},k} \le \tau_{\text{ice,WOT}}(\omega_{e,k}) \tag{2}$$

$$\omega_{e,\min} \le \omega_{e,k} \le \omega_{e,\max} \tag{3}$$

with ω_e as the rotational speed of the ICE. Both the ICE's drag torque $\tau_{\text{ice,drag}}$ and *wide-open-throttle* net torque $\tau_{\text{ice,WOT}}$ are nonnegative and described by a lookup table as a function of its speed ω_e. The generated net power is equal to

$$P_{\text{ice},k} = \tau_{\text{ice},k}\omega_{e,k}. \tag{4}$$

The fuel consumption is described by a lookup table for the injected fuel mass flow Δm_f, i.e.,

$$\Delta m_{f,k} = \Delta m_f(\tau_{\text{ice},k}, \omega_{e,k}) \qquad \text{(g/s)}. \tag{5}$$

Consequently, if the ICE is not shut off during vehicle standstill, the fuel mass flow is given by $\Delta m_{f,k} = \Delta m_f(0, \omega_{e,\min})$. The overall fuel consumption over a driving cycle of length N and during the standstill periods, respectively, is equal to

$$m_f = \sum_{k=1}^{N} \Delta m_{f,k} \qquad \text{(g)} \tag{6}$$

$$m_{f,0} = \sum_{k=1}^{N} \Delta m_{f,k} \mid_{v_{v,k}=0, a_{v,k}=0} \qquad \text{(g)} \tag{7}$$

with vehicle velocity $v_{v,k}$ and acceleration $a_{v,k}$. For conversion from fuel mass to fuel volume, a density of 753 g/l is used. The combustion efficiency, which is also referred to as *brake-specific fuel consumption*, is defined by

$$\beta_{\text{ice},k} = 3.6 \cdot 10^6 \frac{\Delta m_{f,k}}{\tau_{\text{ice},k}\omega_{e,k}} \qquad \text{(g/kWh)}. \tag{8}$$

The combustion efficiency of the ICE is shown in Fig. 3.

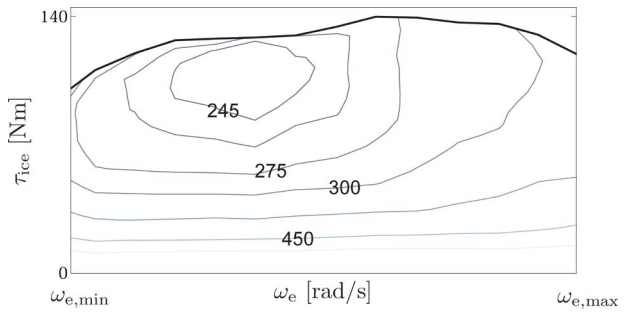

Fig. 3. Combustion efficiency of the engine (in grams per kilowatthour) as a function of engine speed ω_e and generated net torque $\tau_{\rm ice}$.

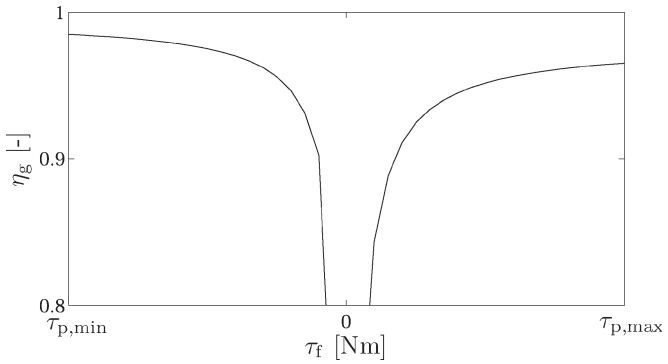

Fig. 4. Flywheel gear transmission efficiency as a function of the applied torque.

B. Flywheel

The FS model is modeled by an inertia $J_{\rm fs}$ on which two torques are acting: the drag torque $\tau_{\rm fs,drag}$ and the torque on the output shaft τ_f, which depends on the selected driving mode (see Section III-A). The dynamics and constraints are given by

$$\omega_{f,k+1} = \omega_{f,k} + \frac{r_g^2}{J_{\rm fs}}\left(-\frac{\tau_{f,k}}{\eta_{g,k}} - \tau_{\rm fs,drag}, kr_g\right)\Delta t \quad (9)$$

$$\tau_{\rm fs,drag,k} = \tau_{\rm fs,drag}(\omega_{f,k}) \quad (10)$$

$$\omega_{f,\min} \leq \omega_{f,k} \leq \omega_{f,\max} \quad (11)$$

with ω_f as the rotational speed of the flywheel clutch. Here, $\tau_{\rm fs,drag}(\omega_f)$ is modeled as a second-order polynomial for positive speeds using nonnegative coefficients based on experimental results, as shortly described in [5], and is equal to zero at zero speed. This drag torque describes the total losses of the system, including bearing, seal, and air drag losses. Note that no explicit constraints apply to τ_f, but they are implicitly given by torque constraints on the CVT. The gear gives a constant gear ratio r_g between ω_f and the rotor and has transmission efficiency η_g, which is described by a lookup table, i.e.,

$$\eta_{g,k} = \begin{cases} \eta_g(\tau_{f,k}), & \text{if } \tau_{f,k} \geq 0 \\ \frac{1}{\eta_g(\tau_{f,k})}, & \text{if } \tau_{f,k} < 0. \end{cases} \quad (12)$$

The flywheel gear transmission efficiency is shown in Fig. 4. The power losses that appear due to the drag torque and the transmission efficiency of the gear, respectively, are given by

$$P_{{\rm drag},k} = \tau_{{\rm fs,drag},k}\omega_{f,k} \quad (13)$$

$$P_{{\rm gear},k} = (1-\eta_{g,k})\tau_{f,k}\omega_{f,k}. \quad (14)$$

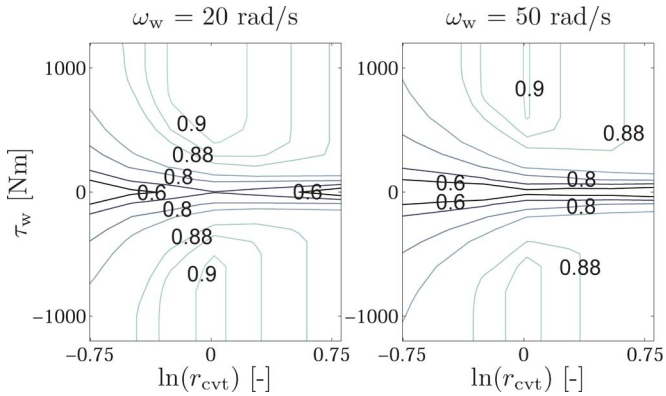

Fig. 5. CVT transmission efficiency as a function of the speed ratio for two different output speeds. (Left) $\omega_w = 20$ rad/s. (Right) $\omega_w = 50$ rad/s.

The energy content of the FS is equal to

$$E_{{\rm fs},k} = \frac{J_{\rm fs}}{2r_g^2}\omega_{f,k}^2. \quad (15)$$

C. CVT

The CVT provides a continuously variable speed ratio $r_{\rm cvt}$ between the primary (subscript p) and secondary pulley shaft (subscript s). Furthermore, the final drive gives a constant speed ratio r_d between the secondary pulley shaft and the wheel shaft (subscript w). Recall that, for the CVT, no inertia is taken into account; the corresponding speed ω and torque τ relations are given by

$$\omega_{p,k} = \frac{\omega_{w,k}}{r_{{\rm cvt},k}r_d} \quad (16)$$

$$\tau_{p,k} = r_{{\rm cvt},k}r_d\frac{\tau_{w,k}}{\eta_{{\rm cvt},k}}. \quad (17)$$

Here, the transmission efficiency of the CVT system $\eta_{\rm cvt}$ is described by a lookup table, i.e.,

$$\eta_{{\rm cvt},k} = \begin{cases} \eta_{\rm cvt}(\omega_{w,k}, \tau_{w,k}, r_{{\rm cvt},k}), & \text{if } \tau_{w,k} \geq 0 \\ \frac{1}{\eta_{\rm cvt}(\omega_{w,k}, \tau_{w,k}, r_{{\rm cvt},k})}, & \text{if } \tau_{w,k} < 0 \end{cases} \quad (18)$$

based on experiments described in [24]. The transmission efficiency includes losses by the pump and final drive using a conventional control strategy for the pressures on the pulley sheaves. Fig. 5 shows the efficiency map for two different values of ω_w. For the simulations, maps of more values for ω_w are used. The power loss is given by

$$P_{{\rm cvt},k} = \left|(1-\eta_{{\rm cvt},k})(\tau_{p,k}\omega_{p,k})\right|. \quad (19)$$

The speed ratio dynamics are described as follows:

$$r_{{\rm cvt},k+1} = r_{{\rm cvt},k} + \Delta r_{{\rm cvt},k}\Delta t. \quad (20)$$

Constraints apply to the speed ratio and primary torque, i.e.,

$$r_{\rm cvt,min} \leq r_{cvt,k} \leq r_{\rm cvt,max} \quad (21)$$

$$\tau_{p,\min} \leq \tau_{p,k} \leq \tau_{p,\max}. \quad (22)$$

Shift speed $\Delta r_{{\rm cvt},k}$ is not constrained to reduce the number of states required to describe the powertrain model. It is assumed

that the CVT does not require higher shift speeds to accelerate or decelerate the FS than is conventionally necessary for the ICE, because of the relatively high inertia of the FS. The required shift forces, however, may be higher and may limit the shift speed; this effect is not considered in this paper.

D. Clutches

The hybrid powertrain contains three actively controlled clutches: the *engine clutch* (subscript e), *flywheel clutch* (subscript f), and *drive clutch* (subscript d). The engine and flywheel clutch are compact and only suitable to synchronize the intermediate shaft between all clutches and to crank the ICE, respectively. These clutches will be used to select different driving modes of the powertrain, as will be described in Section III-A. It is assumed that these clutches engage or disengage within one time step (i.e., 1 s), which is sufficient to synchronize the intermediate shaft or to crank the ICE. Then, the clutches can be modeled by two discrete states, i.e.,

$$C_i := \begin{cases} 0, & \Longleftrightarrow \text{disengaged} \\ 1, & \Longleftrightarrow \text{engaged} \end{cases}, \qquad i \in \{e, f\}. \tag{23}$$

The drive clutch has conventional dimensions and will be only used to launch the vehicle, which may take several time steps. During such a launch, the CVT speed ratio is kept in its lowest gear, and the drive clutch is used to transmit torque τ_p while slipping with slip speed ω_c, which depends on the engaged mover (i.e., clutch states C_e and C_f), according to

$$\omega_{c,k} = \begin{cases} \omega_{e,k} - \omega_{p,k}, & \text{if } C_e = 1 \\ \omega_{f,k} - \omega_{p,k}, & \text{if } C_f = 1. \end{cases} \tag{24}$$

Notice that, when $C_f = C_e = 1$, $\omega_f = \omega_e$ holds. The drive clutch engages as soon as the velocity of the vehicle synchronizes with the rotational speed of the engaged mover, i.e., the FS, and/or the ICE. While slipping, the dissipated power is equal to

$$P_{\text{clutch},k} = |\tau_{p,k}\omega_{c,k}|. \tag{25}$$

E. Vehicle

The vehicle is modeled by an inertia J_w, which is equivalent to the mass of the vehicle, two passengers of 75 kg, and the inertia of all wheels together. Three torques act on this inertia: drag torque $\tau_{w,\text{drag}}$, propulsion torque τ_w, and braking torque $\tau_{w,\text{brake}}$ by the disc brakes. The effective wheel radius R_w, while neglecting any wheel slip, gives a constant speed ratio between the velocity of the vehicle and the rotational speed of the wheels. For a given velocity of the vehicle v_v and acceleration a_v, the speed ω_w and the propulsion torque τ_w at the wheels can be derived as follows:

$$\omega_{w,k} = \frac{v_{v,k}}{R_w} \tag{26}$$

$$\tau_{w,k} = \tau_{w,\text{drag},k} + \frac{J_w}{R_w} a_{v,k} + \tau_{w,\text{brake},k} \tag{27}$$

$$\tau_{w,\text{drag},k} = \tau_{w,\text{drag}}(v_{v,k}). \tag{28}$$

Here, $\tau_{w,\text{drag}}(v_v)$ is modeled as a second-order polynomial for positive velocity using nonnegative coefficients based on estimated parameters of the vehicle and is equal to zero at standstill.

III. Powertrain Model

The hybrid powertrain model, as shown in Fig. 2, can be operated in several driving modes depending on the states of the engine and flywheel clutch. This section explains each relevant driving mode and introduces system variables, i.e., control inputs, system states, and system disturbances, to describe the model and driving cycle in a format suitable for optimization. Furthermore, switches between driving modes are presented, with the corresponding actions of the powertrain. Finally, constraints on the control inputs of the powertrain are introduced to avoid uncomfortable situations. In the sequel, it is assumed that the velocity and acceleration of the vehicle are known in advance, according to the selected driving cycle.

A. Driving Modes

Three relevant driving modes are identified, in which the engine and flywheel clutch are not slipping (i.e., they can be either disengaged or engaged). Here, driving mode ϕ is defined by the states of these clutches (C_e, C_f), i.e.,

$$\phi(C_e, C_f) := \begin{cases} 1, & \Longleftrightarrow\ C_e = 0,\ C_f = 1 \\ 2, & \Longleftrightarrow\ C_e = 1,\ C_f = 1 \\ 3, & \Longleftrightarrow\ C_e = 1,\ C_f = 0. \end{cases} \tag{29}$$

With this definition, the driving mode decides which mover is used to propel the vehicle: either the FS ($\phi = 1$), the ICE ($\phi = 3$), or both ($\phi = 2$). Notice that the driving mode does *not* depend on drive clutch state C_d as this clutch is only used to launch the vehicle from standstill, not to switch between movers. In the following sections, each driving mode is explained in more detail.

1) FS Driving ($\phi = 1$): The CVT is used to either propel or brake the vehicle with the FS while the ICE is disengaged and remains shut off. Within this mode, fuel consumption is reduced by idle-stop by driving on the FS with the ICE shutoff and by BER for later use. The powertrain dynamics are determined by the prescribed driving cycle; thus, the shift speed of the CVT Δr_{cvt} follows implicitly. The braking power of the FS is equal to

$$P_{\text{BER}} = |\tau_{w,k}|\omega_{w,k}|_{\tau_{w,k}<0} \tag{30}$$

whereas the brake torque is distributed between the FS and disc brakes as follows:

$$(1-\gamma)\tau_{w,k} + \gamma\tau_{w,\text{brake},k} = \tau_{w,\text{drag},k} + \frac{J_w}{R_w} a_{v,k} \tag{31}$$

with $0 \le \gamma \le 1$ as the relative amount of braking power applied by the disc brakes. The selection of a suitable value for this parameter is discussed next.

Ideally, all available brake energy is recuperated by the FS. This is, however, not always possible as the FS can only brake

the front wheels; this may lead to vehicle instability at high decelerations. In [25] and [26], it is shown that, for low decelerations (up to -2 m/s^2), still 100% of the brake torque may be applied by the front wheels according to European regulations. However, for medium decelerations up to -4 m/s^2 (the maximum deceleration seen in most driving cycles), the front wheels may apply only 90% of the brake torque. Another requirement to maximize BER is the use of a certified brake–blend (or brake–assist) system, which safely intervenes between the brake pedal and the disc brakes to provide the desired torque split for braking [27]. In this paper, to keep the cost potential of the FS low, the use of such a system is omitted, and a different strategy is chosen: without intervening in the braking system, the FS applies a brake torque *in addition* to the disc brakes.[1] As a consequence, the driver will experience a higher brake pedal sensitivity (pedal force to vehicle deceleration)—this is expected to be acceptable as large variations in pedal sensitivity are already seen between different vehicles, e.g., a factor of 9 for low decelerations in [28]. Nevertheless, increasing the brake pedal sensitivity is limited, such that not all, but still a large portion of the available brake energy can be recuperated. This paper assumes that for decelerations up to -4 m/s^2 (all decelerations in the considered driving cycles), it is sufficient to apply 33% ($\gamma = 0.33$) of the brake torque by the disc brakes for vehicle stability and an acceptable brake pedal sensitivity. When the FS reaches its maximum capacity, all braking power is provided by the disc brakes ($\gamma = 1$).

2) FS Charging ($\phi = 2$)*:* The ICE propels the vehicle while, simultaneously, the FS is "charged" ($\tau_f < 0$) or "discharged" ($\tau_f > 0$) to assist the ICE. The power split depends on the operation point of the ICE, which can be controlled with either τ_{ice} or $(\Delta)r_{\mathrm{cvt}}$. Within this mode, inefficient part-load operation of the ICE is reduced by charging the FS while propelling the vehicle at efficient operation points of the ICE. Vehicle braking in this driving mode is possible but not supported; it is more efficient to recuperate brake energy without the drag torque of the ICE in mode $\phi = 1$.

3) ICE Driving ($\phi = 3$)*:* The ICE propels the vehicle while the FS is disengaged and might be spinning. The operation point of the ICE can be controlled with either τ_{ice} or $(\Delta)r_{\mathrm{cvt}}$. The disc brakes are used to brake the vehicle (i.e., $\tau_{w,k} = 0$), where braking torque $\tau_{w,\mathrm{brake}}$ is determined by the prescribed driving cycle. Within this mode, the vehicle is propelled with conventional performance and fuel consumption—the fuel consumption is not reduced.

Note that for driving modes $\phi \in \{2, 3\}$, an additional control degree of freedom exists, describing the operation of the ICE. This control degree of freedom disappears for $\phi = 1$ as the ICE is shut off. The required propulsion torque(s) from the mover(s), as well as the corresponding speed ratios of the CVT, are summarized for each driving mode in Table II. For some driving-mode switches, an additional torque is required, which is denoted by $\tau_{e,\mathrm{switch}}$ or $\tau_{f,\mathrm{switch}}$, as will be derived in Sections III-C and IV-A, and is equal to zero when no switch takes place.

[1]The effects on the *antilock braking system* need further investigation.

TABLE II
POWERTRAIN OPERATION DURING VARIOUS DRIVING MODES

ϕ	description	τ_{e}^1	τ_{f}^1	r_{cvt}^1
1	FS Driving	0	τ_{p}	$\omega_{\mathrm{s}}/\omega_{\mathrm{f}}$
2	FS Charging	$\tau_{\mathrm{p}} - \tau_{\mathrm{f}}$	$\tau_{\mathrm{p}} - \tau_{\mathrm{e}} + \tau_{\mathrm{f,switch}}$	$\omega_{\mathrm{s}}/\omega_{\mathrm{f}}$
3	ICE Driving	$\tau_{\mathrm{p}} + \tau_{\mathrm{e,switch}}$	$\tau_{\mathrm{f,switch}}$	$\omega_{\mathrm{s}}/\omega_{\mathrm{e}}$

[1]Constraints apply, cf. (2), (3), (11), (21), (22), (38), and (39).

B. Selection of System Variables

For a predefined driving cycle, the hybrid powertrain can be controlled with two control inputs, i.e., $u = [u_1, u_2]^T$, which control both the driving-mode switches and the power split between the FS and the vehicle, respectively. The following control inputs are selected: u_1 controls the driving modes by prescribing the driving mode at the next time sample ϕ_{k+1}, and u_2 controls the operation point of the ICE at current time, with either τ_{ice} or Δr_{cvt}. Here, τ_{ice} is selected, which seems logical from a physical point of view; this degree of freedom only exists when the ICE is engaged, i.e., there is no control degree of freedom with FS Driving. When using τ_{ice} as a control input, the powertrain dynamics and the predefined driving cycle determine shift speed Δr_{cvt} implicitly. The control input vector is defined by

$$u_k := [\phi_{k+1}, \tau_{\mathrm{ice},k}]^T. \tag{32}$$

The hybrid powertrain dynamics can be described with three system states, i.e., $x_k = [x_1, x_2, x_3]^T$. The states are related to the FS dynamics (9), the ICE dynamics (1), and the driving-mode switches. The following states are selected: the FS's energy content E_{fs} (ω_f is also suitable), the ICE's speed ω_e, and current driving mode ϕ_k, i.e.,

$$x_k := [\phi_k, E_{\mathrm{fs},k}, \omega_{e,k}]^T. \tag{33}$$

With *current* driving mode ϕ_k (i.e., x_3) and *next* driving mode ϕ_{k+1} (i.e., u_1), each driving-mode switch is described. The predefined driving cycle can be written as a disturbance acting on the hybrid powertrain model, which is defined by

$$w_k := [v_{v,k}, a_{v,k}]^T. \tag{34}$$

Now, the total system can be written as

$$x_{k+1} = f(x_k, u_k, w_k). \tag{35}$$

C. Switching Between Driving Modes

There are six different switches possible between the three driving modes. Each switch corresponds to one or two actions performed by the powertrain; some switches are constrained under certain conditions, as summarized in Table III. Recall that each switch takes one time step, and while switching from one mode to another, torque is transmitted through the powertrain to propel or to brake the vehicle.

Each action is explained in the following discussion.

1) ICE Start: This paper assumes that the FS always contains sufficient energy to crank the ICE. Furthermore, it is

TABLE III
SWITCHES BETWEEN DRIVING MODES

ϕ_k	ϕ_{k+1}	action	constraint
1	2	ICE Start	High-freq. Switching (41)
1	3	ICE Start & Disengage FS	-
2	1	Disengage ICE	-
2	3	Disengage FS	-
3	1	Sync. FS & Disengage ICE	Difficult Sync. (40)
3	2	Synchronize FS	Difficult Sync. (40)

assumed that the ICE can be cranked smoothly; the driver does not feel it. The additional torque $\tau_{f,switch}$ to crank the ICE from $\omega_{e,k} = 0$ rad/s to $\omega_{e,k+1} = \omega_{f,k}$ rad/s, within one time step, is provided by the FS through the slipping engine clutch and is modeled as

$$\tau_{f,\mathrm{switch},k} = J_{\mathrm{ice}} \frac{\omega_{e,k+1} - \omega_{e,k}}{\Delta t} + \tau_{\mathrm{ice,drag}}(\omega_{e,k+1}). \quad (36)$$

The power loss to crank the ICE is then given by

$$P_{\mathrm{crank},k} = \tau_{f,\mathrm{switch},k} \omega_{f,k}. \quad (37)$$

2) Disengage: when a mover is disengaged, it is assumed that no power is dissipated, and the clutches do not introduce any additional drag torques. Notice that, when the FS is disengaged, additional torque τ_{ice} might be required to change the operation point of the ICE (i.e., ω_e), as described by its dynamics in (1).

3) Synchronize: The CVT is used to synchronize the speeds of both movers for a smooth switch in between; hence, virtually, no power is dissipated. This synchronization, however, may give comfort issues as explained in the following discussion.

D. Comfort-Related Constraints

For the design of the optimal EMS, additional constraints are defined to avoid uncomfortable situations, such as "difficult" clutch synchronization and unexpected noise produced by the ICE. These issues are related to the typical mechanical characteristics of this powertrain: a relatively small energy storage capacity, discrete switches between driving modes, and relatively many kinematic constraints.

1) ICE Assist: In the FS charging mode ($\phi = 2$), when the vehicle is propelled by the ICE ($\tau_w \geq 0$), the FS can be used to assist the ICE to increase the acceleration performance. This functionality, however, is not supported because the ICE decelerates together with the FS due to the mechanical connection in between. A decelerating ICE implies the following: 1) a decreasing ICE power, thereby requiring increasing assistance, which is limited by the energy storage capacity of the FS; when the FS is "depleted," the ICE can only deliver very limited power as it runs at low speed; and 2) a decreasing ICE noise frequency, whereas the driver expects an increasing noise frequency with high power demand. These issues are expected to be unacceptable; hence, ICE assist is not supported, as indicated by the following constraint:

$$u_{2,k} \in \{\tau_{\mathrm{ice},k} \mid \tau_{f,k}(x_k, u_k, w_k) \leq 0, \tau_{w,k} \geq 0\}. \quad (38)$$

In this mode, vehicle braking ($\tau_w < 0$) is also not supported, as it is more efficient to recuperate brake energy without the drag torque of the ICE in mode $\phi = 1$; if not possible, only the disc brakes are used, which is a functionality of mode $\phi = 3$. The corresponding constraint is given by

$$u_{1,k} \in \{\phi \mid \phi_k \neq 2, \quad \tau_{w,k} < 0\}. \quad (39)$$

2) Difficult Synchronization: When switching from ICE Driving ($\phi = 3$) to FS Charging ($\phi = 2$) or to FS Driving ($\phi = 1$), the ICE speed needs to be synchronized with the FS speed, such that the flywheel clutch can be engaged. When the ICE propels the vehicle $\tau_w \geq 0$, this switch is possible by changing the speed ratio of the CVT until the ICE and FS speeds synchronize. This synchronization, however, may take a relatively long time for two reasons: 1) The switch speed of the CVT is relatively slow, and 2) the synchronization has to be very accurate to avoid a torque peak caused by the relatively large inertia of the FS during quick engagement of the flywheel clutch (which is not designed to dissipate much energy). In addition, the sudden change in ICE speed gives an unexpected change in ICE noise frequency. From a driver's comfort point of view, the powertrain has to be able to respond within an acceptable time frame, e.g., within 1 s, and without sudden changes in the ICE noise. To avoid these issues, this driving-mode switch is not supported, as indicated by the following constraint:

$$u_1 \in \{\phi \mid \phi_{k+1} = 3, \quad \phi_k = 3, \quad \tau_{w,k} \geq 0\}. \quad (40)$$

When the vehicle brakes ($\tau_w < 0$), the situation is different. During this switch, it is assumed that the disc brakes decelerate the vehicle; no power is transmitted through the CVT. The drive clutch can be disengaged, and subsequently, the flywheel clutch can be engaged to synchronize the intermediate shaft with the FS. Then, the "unloaded" CVT can quickly switch to the desired speed ratio, whereas the drive clutch can be used for a smooth synchronization. This switch allows for BER after ICE Driving. Note that only switching toward $\phi = 1$ is allowed since switching toward $\phi = 2$ when braking is constrained by (39).

3) High-Frequent Switching: Alternating between FS Driving and FS Charging might be a fuel-efficient way to propel the vehicle at a constant velocity. The corresponding switching frequency depends on the energy storage capacity of the FS—the energy storage capacity is relatively small. Moreover, the switching frequency increases with the velocity of the vehicle. A high switching frequency, however, is expected to be uncomfortable for the driver due to the constantly changing noise of the ICE, whereas the velocity of the vehicle remains constant. This high-frequent switching is already penalized with a *soft* constraint by taking the power loss into account for cranking the ICE [cf. (36)]. In addition, a *hard* constraint is introduced as follows:

$$u_1 \in \{\phi \mid \phi_{k+1} \neq 2, \phi_k = 1, v_{\mathrm{v},k} > v_{\mathrm{c}}, |a_{\mathrm{v},k}| < a_{\mathrm{c}}\} \quad (41)$$

with nonnegative coefficients v_c (m/s) and a_c (m/s^2), which define a "constant" high velocity. With this constraint, FS

Charging is not allowed at high constant velocities. FS Driving, however, is still supported to enable usage of "free" recuperated brake energy.

IV. Optimization

The control objective is to minimize the overall fuel consumption over a predefined driving cycle of length N, i.e.,

$$\min_{u_k} \sum_{k=1}^{N} \Delta m_f(x_k, u_k, w_k)\Delta t \tag{42}$$

subject to

- system's kinematics and dynamics: see (1), (9), (16), (17), (20), (23), (26), (27), and (29);
- system's constraints: see (2), (3), (11), (21), and (22);
- comfort-related constraints: see (38)–(41);
- end-value constraint: $E_{\mathrm{fs}}(N) = E_{\mathrm{fs}}(1)$.

The end-value constraint is introduced to assure a zero net-energy balance of the FS over the total driving cycle. The signal flow of this optimization problem is schematically depicted in Fig. 1: with control inputs τ_{ice} and ϕ (i.e., clutch states C_e and C_f), disturbances v_v and a_v, and output Δm_f. This section describes an approach to numerically solve the optimization problem written earlier.

A. Problem Reductions

The optimization problem described by (42) consists of two control inputs (32), three state variables (33), and a driving cycle of length N. The computational complexity of the optimization problem exponentially increases with the number of control inputs, number of state variables, and length of the driving cycle [8]. Consequently, the computation time to solve this optimization problem is relatively long. To reduce the computational complexity, three methods are proposed to reduce the number of control inputs and state variables.

1) Combining Control Inputs: Control input u_2 (i.e., τ_{ice}) is only defined for $u_1 = \{\phi(2), \phi(3)\}$—for $\phi(1)$ (i.e., FS Driving), τ_{ice} is undefined because the ICE is shut off. Hence, for finite row length M_{u2} of discrete control input u_2, the two control inputs may be combined into one, i.e.,

$$u = \left[\phi(1), \begin{bmatrix} \phi(2) & \cdots & \phi(2) \\ \tau_{\mathrm{ice}}(1) & \cdots & \tau_{\mathrm{ice}}(M_{u2}) \end{bmatrix} \begin{bmatrix} \phi(3) & \cdots & \phi(3) \\ \tau_{\mathrm{ice}}(1) & \cdots & \tau_{\mathrm{ice}}(M_{u2}) \end{bmatrix}\right]. \tag{43}$$

The row length of control input u_1 is equal to $M_{u1} = 3$. Now, using (43), the number of discrete control input combinations U reduces from $U = M_{u1}M_{u2} = 3M_{u2}$ for independent u_1 and u_2 to $U = 2M_{u2} + 1$ for (43).

2) A priori Optimization 1: For $u_1 = \phi(3)$ (i.e., ICE Driving), two assumptions are made.

1) Optimal control input u_2 (i.e., τ_{ice}) is independent of optimal control input u_1 (i.e., ϕ). This assumption seems reasonable because, as with ICE Driving, the two optimization problems are independent: τ_{ice} optimizes operation point of the ICE without influencing FS's energy content E_{fs}, whereas ϕ uses E_{fs} to optimize the overall fuel consumption.
2) The optimal ICE speed changes very slowly; thereby, the required torque to accelerate its inertia is negligible. The remainder of the powertrain can still be in transient condition; the vehicle, in particular, is allowed to accelerate or decelerate. This assumption is often found in the literature and seems reasonable with fuel-optimal operation of the ICE [29], [30].

After that, the optimization problem can be reduced in two ways: 1) Omit control input u_2 for $\phi = 3$ by calculating the statically optimal τ_{ice} for each $\{x, w\}$ *a priori*, with

$$\tau_{\mathrm{ice},k} = \arg\min_{\tau_{\mathrm{ice},k}} \Delta m_f(x_k, u_k, w_k) \mid_{\phi_k = 3} \tag{44}$$

and 2) omit state x_2 (i.e., ω_e) and simplify the ICE dynamics described by (1) to

$$\omega_{e,k} = \frac{\tau_w \omega_w}{\eta_{\mathrm{cvt},k}\tau_{e,k}}. \tag{45}$$

The dynamics of the ICE between driving-mode switches are not omitted; in these dynamic situations, accelerations of the ICE might be significant. Between driving-mode switches, accelerations can be calculated without x_2 since ω_e is determined for each driving mode: $\omega_e = 0$ rad/s for $\phi = 1$, $\omega_e = \omega_f$ for $\phi = 2$, and (45) holds for $\phi = 3$. The torque needed to accelerate the ICE during a driving-mode switch is equal to

$$\tau_{e,\mathrm{switch},k} = J_{\mathrm{ice}} \frac{\omega_{e,k+1} - \omega_{e,k}}{\Delta t}. \tag{46}$$

This *a priori* optimization results in a static fuel-optimal operation of the ICE and CVT during ICE Driving, which is also referred to as *optimal operation line* tracking [31]. Combining (43)–(45), the optimization problem is reduced as follows: 1) the number of discrete control input combinations is reduced to $U = M_{u2} + 2$, whereas 2) the number of discrete state combinations X reduces from $X = M_{x1}M_{x2}M_{x3} = 3M_{x2}M_{x3}$ to $X = 3M_{x2}$, with $M_{x1} = 3$ as the row length of state vector x_1 and finite vector lengths M_{x2} and M_{x3} for x_2 and x_3, respectively.

3) A priori Optimization 2: For $u_1 = \phi(2)$ (i.e., FS Charging), two assumptions are made.

1) Optimal control input u_2 is independent of optimal control input u_1. This is a severe assumption, as with FS Charging, E_{fs} is directly influenced by τ_{ice}, whereas ϕ uses E_{fs} to optimize the overall fuel consumption. By optimizing τ_{ice} without considering the energy balance of the system, a suboptimal solution is found. In the sequel, the impact of this assumption is investigated.
2) Optimal τ_{ice}, which minimizes the overall fuel consumption, is close to τ_{ice} that maximizes ICE efficiency β_{ice}.

After that, the optimization problem can be reduced as follows: Omit control input u_2 for $\phi = 2$, by calculating the statically optimal τ_{ice} for each $\{x, w\}$ *a priori:*

$$\tau_{\mathrm{ice},k} = \arg\max_{\tau_{\mathrm{ice},k}} \beta_{\mathrm{ice}}(x_k, u_k, w_k) \mid_{\phi_k = 2}. \tag{47}$$

This *a priori* optimization determines the power split statically during FS Charging: For a given FS speed, the ICE speed is determined (mechanically), and the ICE torque that gives the optimal ICE efficiency is selected. Combining (44)–(47), the optimization problem is reduced as follows: 1) The number of discrete control input combinations is reduced to $U = 3$ (only the driving modes), whereas 2) the number of discrete state combinations remains the same as with *A priori Optimization 1*, i.e., $X = 3M_{x2}$.

B. DP

DP is applied to solve the optimization problem with a numerical algorithm that follows three steps: 1) The continuous optimization problem is discretized; 2) for each state x, control input u, and disturbance w, the cost function is evaluated and stored in a cost matrix; and 3) a systematic routine based on Bellman's principle of optimality [11] is used to find the global optimal solution for a predefined driving cycle w using the precalculated cost matrix. The following optimization problems are considered:

- problem (42) reduced by –(45) (*DP1*);
- problem (42) reduced by –(47) (*DP2*).

Both DP1 and DP2 optimize the driving-mode sequence dynamically. The difference lies in the optimization of the power split (ICE torque) with FS Charging: DP1 optimizes the power split dynamically, whereas DP2 optimizes the power split statically (*a priori*). For comparison reasons, the fuel consumption of the baseline vehicle without FS (*BL*) is computed using reductions (44) and (45), with restricted control input $\phi_{k+1} = 3$. The same model is used, including the FS mass of 27 kg, of which its effect on the fuel consumption is expected to be negligible. Note that all optimizations (DP1, DP2, and BL) use the same model and the same static *a priori* optimization of the ICE torque with ICE Driving (44), so that clear comparisons can be made with respect to the type of the power-split optimization (static or dynamic) and FS usage.

C. Discretization of Variables

The reduced optimization problems DP1 and DP2 are described with two states, i.e., $x = [E_{\mathrm{fs},k}, \phi_k]^T$, and one or two control inputs, i.e., $u = [\phi_{k+1}, \tau_{\mathrm{ice},k}]^T$ for DP1 and $u = [\phi_{k+1}]$ for DP2, respectively. The continuous variables are linearly discretized, with discretization steps of $\Delta E_{\mathrm{fs}} = 100$ J for x and $\Delta\alpha = 0.05$ for u_2. Here, $0 \leq \alpha \leq 1$ is selected as an indirect control input for τ_{ice}; α represents the fraction of the torque reserve and describes the generated net torque of the ICE by

$$\tau_{\mathrm{ice},k} = \alpha(\tau_{\mathrm{WOT},k} - \tau_{p,k}) + \tau_{p,k}. \tag{48}$$

Recall that ϕ is already discrete, with three driving modes.

D. Cost Matrix

The cost matrix needs to be computed for each value of w (i.e., $[v_v, a_v]^T$) that occurs in a driving cycle. A straightforward way to implement this in the algorithm is to evaluate the cost function for each time sample of the driving cycle. A more efficient implementation, however, is to evaluate only the *unique* values for w in a driving cycle. This implementation can save almost 50% on computational costs for the considered set of driving cycles, as shown in Table IV. The driving cycles themselves are described next.

TABLE IV
NUMBER OF UNIQUE SAMPLES IN THE DRIVING CYCLES

Driving cycle	Time samples [-]	Unique samples [-]	Reduction
NEDC	1180	245	−79.2 %
CADC	2075	1547	−25.5 %
FTP75	1877	938	−50.0 %
JC08	1377	791	−42.6 %
JP1015	661	159	−75.9 %
Hurk	879	698	−20.6 %
total	8049	4378	−45.6 %

E. Driving Cycles

Six driving cycles are considered: the New European Driving Cycle (NEDC), the combined urban and extra urban parts of the Common Artemis Driving Cycle (CADC), thereby omitting the highway part, the Federal Test Procedure 75 (FTP75), the Japan Cycle'08 (JC08), the (older) Japan 10–15 mode (JP1015), and our own real-life driving cycle (Hurk; see Fig. 6). The goal of this paper is to design an optimal EMS for the considered hybrid powertrain under realistic driving conditions. Therefore, in addition to the standard cycles (NEDC, FTP75, JC08, and JP1015), which are widely used for certified fuel consumption measurements, real-world driving cycles are added. The CADC represents real-world driving behavior of passenger cars in Europe [32], whereas the Hurk driving cycle is an actually measured fragment of a more aggressive type of driving. Highway cycles, such as the highway part of the CADC, are omitted since these high-power, high-speed cycles give very limited possibilities for the FS; the added hybrid functionalities, as summarized in Section I, are aimed at urban use.

V. RESULTS AND DISCUSSION

This section first describes and compares the BL, DP1, and DP2 optimization results. These results are compared to answer the following questions: 1) What is the fuel-saving potential of the optimally controlled mechanical hybrid powertrain, and 2) what is the difference in fuel consumption and EMS between DP1 and DP2? Subsequently, the results of DP1 are analyzed to answer the following questions: 3) How does the optimal EMS use the hybrid functionalities, 4) which effects contribute to the increase in transmission losses, and 5) how is the flywheel optimally utilized?

A. Fuel-Saving Potential

Fig. 7 summarizes the fuel consumption results of the BL, DP1, and DP2 optimization problems for the considered six driving cycles. In addition, it shows the fuel-saving results of the hybrid powertrain (i.e., DP1 and DP2) with respect to the conventional powertrain (i.e., BL). It can be seen that, despite

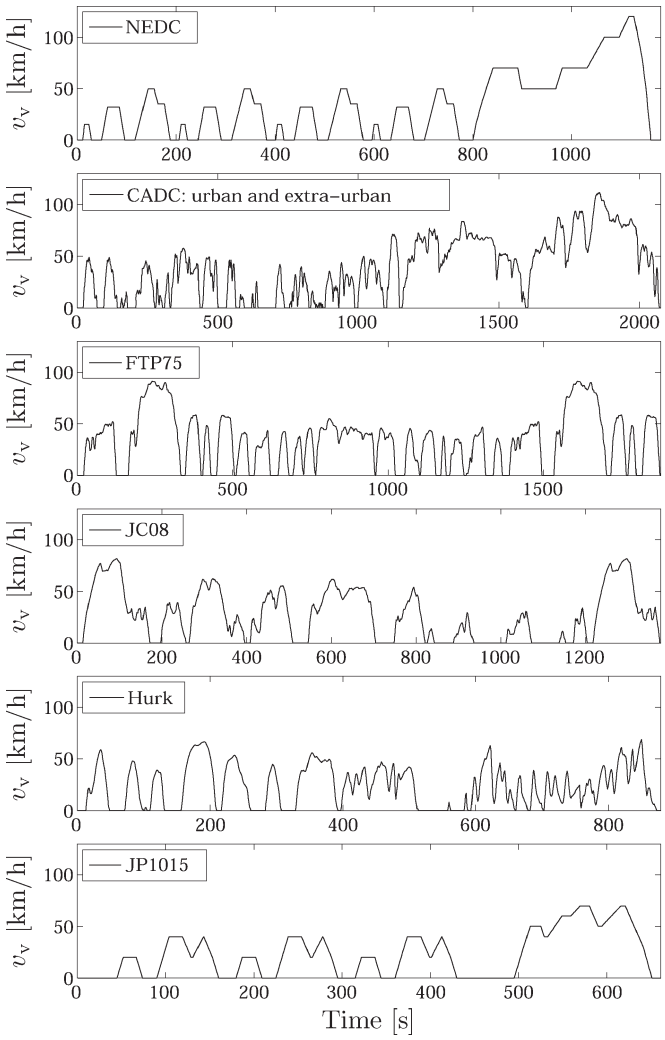

Fig. 6. Six representative driving cycles: NEDC, CADC, FTP75, JC08, Hurk, and JP1015.

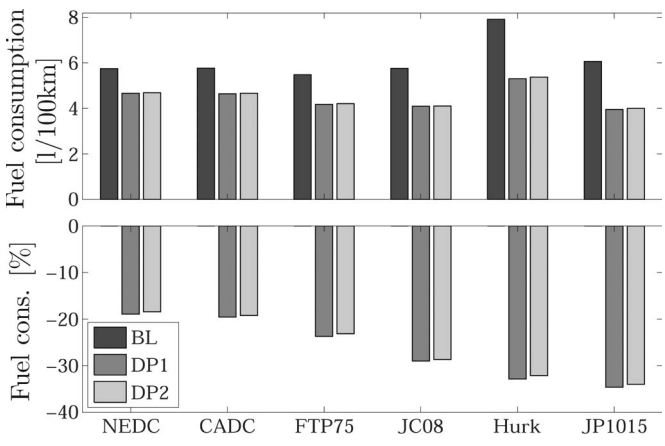

Fig. 7. Results. (Top) Fuel consumption results of the (black) BL, (dark gray) DP1, and (light gray) DP2 optimization problems. (Bottom) Fuel-saving potential results of DP1 and DP2 with respect to the results of BL.

the relatively low energy storage capacity of the FS, a fuel saving can be achieved between 18.4% and 34.7%, which mainly depends on the selected driving cycle. As expected, since the FS is aimed for urban use, a lower fuel saving is achieved with driving cycles that contain extra urban or highway parts, such as the NEDC, CADC, and FTP75. Note that this trend holds for hybrid vehicles in general.

This paper assumes a warm powertrain, whereas the NEDC, CADC, and FTP75 officially start with a cold ICE and transmission. Under cold conditions, the ICE and transmission have lower efficiency values, resulting in higher fuel consumption [33]. For the hybrid powertrain, this effect is expected to be stronger than for the conventional powertrain—due to efficient use of the ICE, e.g., shutoff during standstill, the ICE has a longer warm-up time. On the other hand, due to higher transmission losses of the hybrid powertrain, the transmission has a shorter warm-up time. Overall, it is expected that a significant fuel saving still remains when taking these aspects into account.

Recall that with these calculations, the disc brakes are assumed to absorb 33% of the braking energy [cf. (31)] to avoid the use of a brake–blend system. Simulations with minimal use of the disc brakes (only for vehicle stability) show a slightly higher fuel saving of 1%–5% depending on the driving cycle—although this additional fuel saving is not marginal, it is expected that it does not justify the cost of an additional component (brake–blend system) in the low-cost FS.

B. Problem Reduction

Another observation is that the fuel savings of DP1 and DP2 are very similar; the difference in fuel saving is at most 0.8%. This result suggests that, with a *statically* optimized power split, still a close-to-optimal EMS can be found. Fig. 8 shows the optimal results in more detail for two very different driving cycles: 1) the relatively static NEDC, which contains many constant-velocity parts, low accelerations, and a highway part; and 2) the relatively dynamic Hurk cycle, which contains many and high accelerations and decelerations and no highway part, as shown in Fig. 6. From top to bottom, the seven graphs depict, respectively, the velocity of the vehicle, the optimal driving mode, the optimal net torque of the ICE, the speed ratio of the CVT, the energy content of the FS, the fuel consumption of the ICE, and the power losses due to the slipping drive clutch (25) and cranking of the ICE (37). The results are shown for both DP1 (solid gray line) and DP2 (dashed black line) optimization problems. In this figure, it can be seen that the optimal EMS designs, i.e., optimal driving modes and the ICE's generated net torque, are very similar for DP1 and DP2. This observation correlates with the fuel consumption—the fuel consumption results of DP1 and DP2 are very similar. With DP2, however, the power-split optimization complexity is greatly reduced as it requires no knowledge of the driving cycle. This can be explained as follows: The most efficient way to charge the FS is to operate the ICE at its maximum efficiency, as described by (47) for DP2. For only a few situations, allowing a control degree of freedom with FS Charging (as with DP1) is beneficial to influence the time needed to charge the FS to a desired energy level—an (early) switch to (inefficient) ICE Driving may be avoided (see Fig. 8). Nevertheless, this influence is limited by a small region where the ICE is very efficient (see Fig. 3); thus, its effect on the fuel consumption is small. Next, the effect of each hybrid functionality on the fuel consumption is discussed.

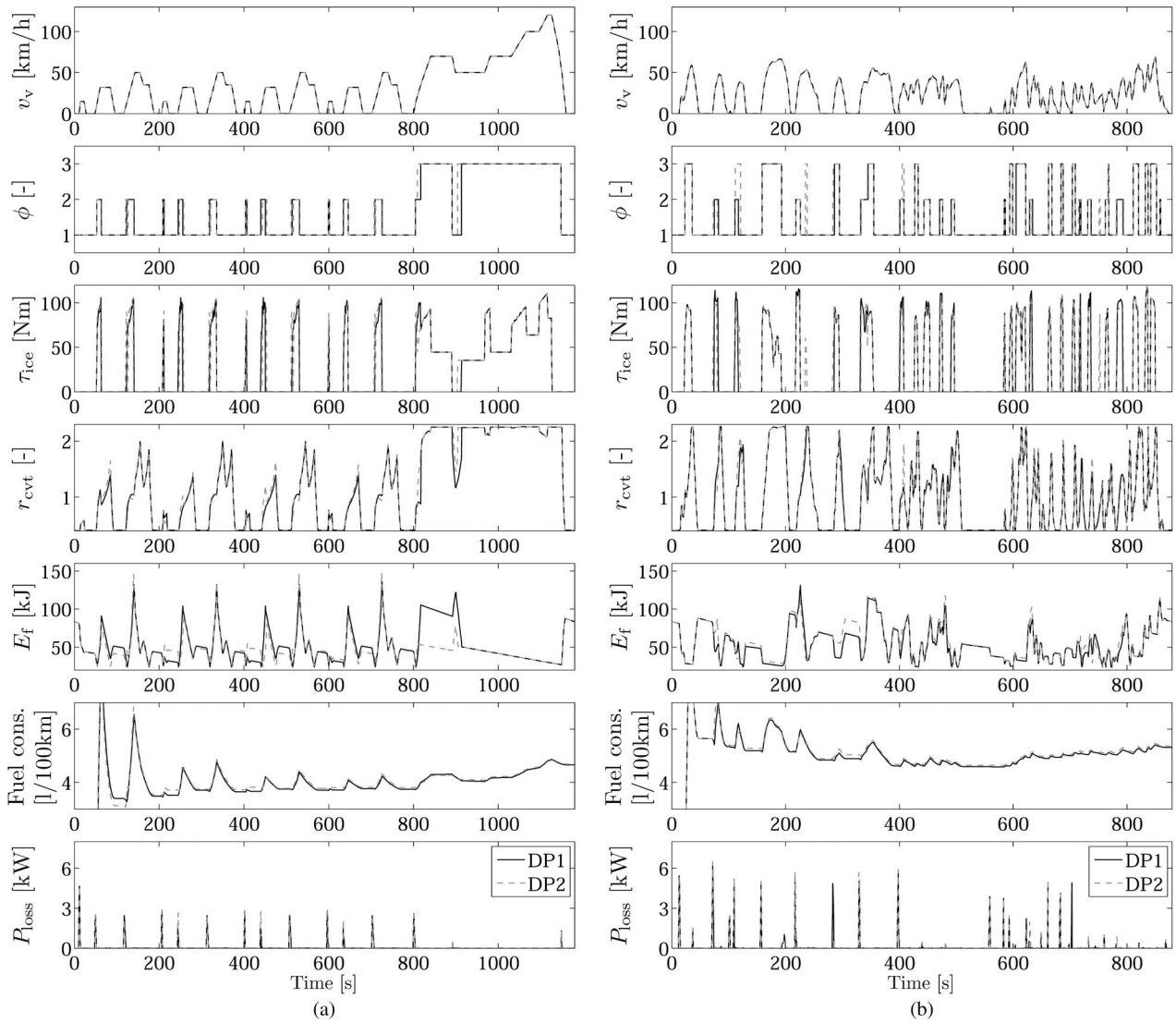

Fig. 8. Results. Solutions of the (solid gray line) DP1 and (dashed black line) DP2 optimization problems for two driving cycles. (Top to bottom) Velocity of vehicle v_v, driving mode ϕ, generated net torque of the ICE τ_{ice}, speed ratio of the CVT r_{cvt}, energy content of the FS E_{fs}, overall fuel consumption, and power losses as a result of ICE cranking and slipping clutches P_{loss}. (a) NEDC. (b) Hurk.

C. Hybrid Functionalities

The hybrid powertrain provides a fuel-saving potential with respect to the conventional powertrain, which can be attributed to the added hybrid functionalities: 1) BER for later use; 2) reduced inefficient part-load operation of the ICE; and 3) idle-stop of the ICE. In Fig. 8, it can be seen that the hybrid functionalities are generally used as follows: at standstill, the ICE is shut off while the FS is spinning; at low velocity and low acceleration, the FS launches the vehicle from standstill and propels the vehicle; at low velocity and medium acceleration, the FS cranks the ICE and the ICE propels the vehicle while charging the FS; at high velocity and/or high acceleration, the ICE propels the vehicle and the FS is disengaged; if possible, the FS brakes the vehicle for BER. With this strategy, the ICE is operated at fuel-efficient (high) torques, except for some parts in the NEDC (between 850 and 1100 s), which can be explained by constraints (40) and (41).

The hybrid functionalities reduce the fuel consumption by two effects: 1) the consumed combustion energy generated by the ICE is reduced by the reuse of brake energy—the added FS, however, generates additional transmission losses, thereby increasing the consumption of combustion energy; and 2) the combustion energy is generated with a higher combustion efficiency due to reduced inefficient part-load operation and shutting off of the ICE during standstill. The effect of each hybrid functionality on the fuel-saving potential of the hybrid powertrain optimized with DP1, with respect to the conventional powertrain (BL), is shown in Fig. 9. In this figure, the increase in fuel consumption corresponds to the increased transmission losses, whereas the decrease in fuel consumption corresponds to the hybrid functionalities.

The results show that, for the reduction in combustion losses, both the increased operation efficiency values of the ICE (10.7%–17.6%) and idle-stop (4.0%–14.3%) are effective. The consumed combustion energy is significantly reduced with BER (8.2%–28.2%)—this effect is, however, largely canceled by the increased transmission losses (8.8%–15.6%), except for the real-life cycle due to the relatively many decelerations.

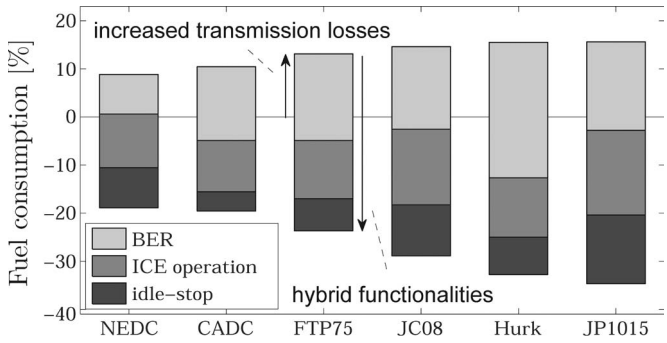

Fig. 9. Results. Effect of each hybrid functionality on the fuel-saving potential of the hybrid powertrain. The higher transmission losses increase the overall fuel consumption, whereas the hybrid functionalities, i.e., 1) BER (light gray), 2) reduction of inefficient ICE operation (dark gray), and 3) idle-stop of the ICE (black), decrease the overall fuel consumption.

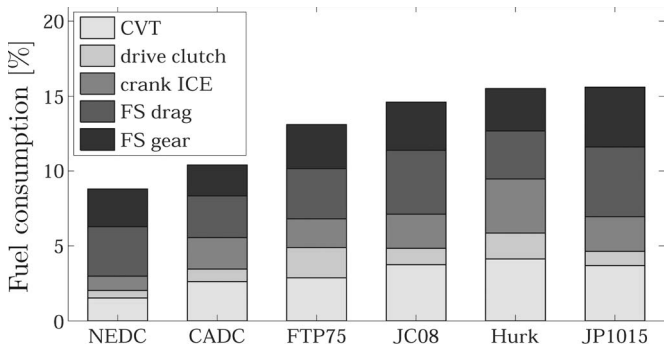

Fig. 10. Results. Effect on the fuel consumption of the higher transmission losses of the CVT, drive clutch, cranking of the ICE, FS drag, and FS gear.

More general, fuel is mainly saved by reduced *combustion losses*, i.e., idle-stop and efficient ICE operation combined (14.7%–31.9%) and, to a lesser extent, by reduced *energy consumption*, i.e., BER and transmission losses combined (−0.6%–12.7%). Overall, it can be concluded that, for this mechanical hybrid powertrain, each of the three hybrid functionalities significantly contributes to the overall fuel saving: ranging from approximately ∼5%–10% for idle-stop to ∼10%–15% for efficient ICE operation and ∼15%–25% for BER. Usage of the FS, however, increases the transmission losses to a great extent, which significantly reduces the fuel saving with approximately ∼10%–15%, such that a fuel-saving potential of ∼20%–35% remains dependent on the driving cycle.

D. Transmission Losses

The additional transmission losses include drag and gear losses in the FS, cranking of the ICE, slipping losses in the drive clutch, and additional transmission losses in the CVT—the hybrid powertrain also uses the CVT during braking (i.e., BER), which is not the case for a conventional powertrain. Fig. 10 zooms in on the increase in fuel consumption due to additional transmission losses of the hybrid powertrain (DP1) with respect to the conventional powertrain (BL). The CVT, FS drag, and FS gear contribute with a similar amount of approximately ∼2%–4% to the total transmission losses; the drive clutch and cranking of the ICE contribute together with a similar amount of ∼2%–4%.

TABLE V
SIMULATION RESULTS OF DP1: OPTIMAL UTILIZATION OF THE FLYWHEEL AND SWITCH FREQUENCIES FOR DRIVING MODES AND ICE CRANKING

	NEDC	CADC	FTP75	JC08	Hurk	JP1015
FS charging source [%]:						
- Brake energy	27.4	54.5	45.4	40.4	70,2	36.9
- ICE energy	72.6	45.5	54.6	59.6	29.8	63.1
Switch-frequency [1/min]:						
- Driving mode	1.37	2.89	2.46	2.48	3.82	2.27
- ICE cranking	0.66	1.30	1.15	1.09	1.84	1.09

E. Flywheel Utilization

Finally, Table V summarizes how the hybrid powertrain is used with the optimal EMS. The FS is used for each driving cycle in a different manner. For example, the relatively static NEDC has many low-power acceleration parts, where the FS is charged with the ICE. The relatively dynamic Hurk cycle, on the other hand, has many decelerations, where the FS is charged with brake energy. Moreover, the driving cycles that are more dynamic (e.g., the Hurk cycle) require higher frequencies for both driving-mode switches and cranking of the ICE than the driving cycles that are more static (e.g., the NEDC cycle).

VI. CONCLUSION

A dynamic simulation model has been presented for a mechanical hybrid powertrain, which supports three hybrid functionalities to reduce fuel consumption: 1) recuperation of brake energy for later use; 2) efficient operation of the engine; and 3) engine shutoff during vehicle standstill. For the design of an optimal EMS, an optimization problem was introduced to minimize the fuel consumption subject to the system's kinematics, dynamics, and constraints. DP was applied to solve both optimization problems for six representative driving cycles. The results show that, with optimal control of the mechanical hybrid powertrain and despite the relatively low energy storage capacity of the flywheel, remarkably high fuel savings of between 18% and 35% can be obtained depending on the selected driving cycle. In addition, with *a priori* (static) optimization of the power distribution for each driving mode, still a close-to-optimal fuel saving is achieved (difference $<$ 0.8%), whereas the complexity of the optimization problem is significantly reduced. Analysis of the results shows that each hybrid functionality contributes with a similar amount to the fuel-saving potential.

REFERENCES

[1] E. Schaltz, A. Khaligh, and P. Rasmussen, "Influence of battery/ultracapacitor energy-storage sizing on battery lifetime in a fuel cell hybrid electric vehicle," *IEEE Trans. Veh. Technol.*, vol. 58, no. 8, pp. 3882–3891, Oct. 2009.
[2] C. Brockbank, "Development of full-toroidal traction drive in flywheel based mechanical hybrids," in *Proc. 6th Int. Conf. Continuously Variable Hybrid Transm.*, Maastricht, The Netherlands, 2010, pp. 163–169.
[3] D. Kok, "Design optimization of a flywheel hybrid vehicle," Ph.D. dissertation, Tech. Univ. Eindhoven, Eindhoven, The Netherlands, 1999.
[4] R. van Druten, "Transmission design of the zero inertia powertrain," Ph.D. dissertation, Tech. Univ. Eindhoven, Eindhoven, The Netherlands, 2001.

[5] B. Vroemen, P. Debal, L. Römers, and M. Maessen, "MecHybrid; a low-cost mechanical hybrid," in *Proc. 6th Int. Conf. Continuously Variable Hybrid Transm.*, Maastricht, Netherlands, 2010, pp. 194–199.
[6] K. van Berkel, L. Römers, B. Vroemen, T. Hofman, and M. Steinbuch, "Performance simulations of a low-cost hybrid powertrain with large fuel savings," *Int. J. Powertrains*, to be published.
[7] T. Hofman, M. Steinbuch, R. van Druten, and A. Serrarens, "Design of CVT-based hybrid passenger cars," *IEEE Trans. Veh. Technol.*, vol. 58, no. 2, pp. 572–587, Feb. 2009.
[8] L. Guzella and S. Sciarreta, *Vehicle Propulsion Systems: Introduction to Modeling and Optimization*, 2nd ed. Berlin, Germany: Springer-Verlag, 2007.
[9] B. Mashadi and S. Emadi, "Dual-mode power-split transmission for hybrid electric vehicles," *IEEE Trans. Veh. Technol.*, vol. 59, no. 7, pp. 3223–3232, Sep. 2010.
[10] S. Delprat, J. Lauber, T. Guerra, and J. Rimaux, "Control of a parallel hybrid powertrain: Optimal control," *IEEE Trans. Veh. Technol.*, vol. 53, no. 3, pp. 872–881, May 2004.
[11] R. Bellman, *Dynamic Programming*. Princeton, NJ: Princeton Univ. Press, 1962.
[12] Y. Zhu, Y. Chen, Z. Wu, and A. Wang, "Optimisation design of an energy management strategy for hybrid vehicles," *Int. J. Alternative Propulsion*, vol. 1, no. 1, pp. 47–62, 2006.
[13] G. Paganelli, G. Ercole, A. Brahma, Y. Guezennec, and G. Rizzoni, "General supervisory control policy for the energy optimization of charge-sustaining hybrid electric vehicles," *JSAE Rev.*, vol. 22, no. 4, pp. 511–518, Oct. 2001.
[14] M. Koot, J. T. B. A. Kessels, B. de Jager, W. P. M. H. Heemels, P. P. J. van den Bosch, and M. Steinbuch, "Energy management strategies for vehicular electric power systems," *IEEE Trans. Veh. Technol.*, vol. 54, no. 3, pp. 771–782, May 2005.
[15] J. Kessels, M. Koot, P. van den Bosch, and D. Kok, "Online energy management for hybrid electric vehicles," *IEEE Trans. Veh. Technol.*, vol. 57, no. 6, pp. 3428–3440, Nov. 2008.
[16] T. van Keulen, B. de Jager, and M. Steinbuch, "An adaptive sub-optimal energy management strategy for hybrid drivetrains," in *Proc. 17th IFAC World Congr.*, Seoul, Korea, 2008, pp. 102–107.
[17] F. Salmasi, "Control strategies for hybrid electric vehicles: Evolution, classification, comparison, and future trends," *IEEE Trans. Veh. Technol.*, vol. 56, no. 5, pp. 2393–2404, Sep. 2007.
[18] S. Wright, "Control of IVT-based vehicles by intelligent selection between alternative solutions," Ph.D. dissertation, Univ. Lancaster, Lancaster, U.K., 2006.
[19] Y. Huang, "A hybrid power driving system with an energy storage flywheel for vehicles," in *Proc. SAE Comm. Veh. Eng. Congr.*, Rosemont, IL, 2007, pp. 1–10.
[20] E. Spijker, "Steering and control of a CVT based hybrid passenger car," Ph.D. dissertation, Tech. Univ. Eindhoven, Eindhoven, The Netherlands, 1994.
[21] C. Wittmer, L. Guzella, and P. Dietrich, "Optimized control strategies for a hybrid car with a heavy flywheel," *Automatisierungstechnik*, vol. 44, no. 7, pp. 331–337, 1996.
[22] D. V. Ngo, T. Hofman, M. Steinbuch, and A. Serrarens, "Optimal shifting strategy for a parallel hybrid electric vehicle," in *Proc. 25th Int. Elect. Vehicle Symp.*, Shenzen, China, 2010, pp. 1–8.
[23] O. Sundstrom, P. Soltic, and L. Guzzella, "A transmission-actuated energy-management strategy," *IEEE Trans. Veh. Technol.*, vol. 59, no. 1, pp. 84–92, Jan. 2010.
[24] K. van Berkel, T. Hofman, B. Vroemen, and M. Steinbuch, "Optimal regenerative braking with a push-belt CVT: An experimental study," in *Proc. 10th Int. Symp. Adv. Veh. Control*, Loughborough, U.K., 2010, pp. 67–72.
[25] M. Ehsani, Y. Gao, and A. Emad, *Modern Electric, Hybrid Electric and Fuel Cell Vehicles: Fundamentals, Theory and Design*, 2nd ed. Boca Raton, FL: CRC, 2005.
[26] J. Hellgren and E. Jonasson, "Maximisation of brake energy regeneration in a hybrid electric parallel car," *Int. J. Elect. Hybrid Veh.*, vol. 1, pp. 95–121, 2007.
[27] A. Kade, A. J. Walenty, and K. G. Leppek, "Regenerative and friction brake blend control," U.S. Patent 5 511 859, 1996.
[28] M. Dodd and I. Knight, "Technical assistance and economic analysis in the field of legislation pertinent to the issue of automotive safety: Provision for information and services on the subject to brake assist systems," Transp. Res. Lab., Manchester, U.K., Client Project Rep. CPR 403, 2007.
[29] C. D. Chan, D. Yang, T. Volz, D. Breitweiser, F. S. Jamzadeh, A. Frank, and T. Omitsu, "System Design and Control Considerations of Automotive Continuously Variable Transmissions," presented at the Conf. SAE Int., Warrendale, PA, 1984, SAE Paper 840048.
[30] S. Liu and B. Paden, "A survey of today's CVT controls," in *Proc. 36th IEEE Conf. Decision Control*, 1997, vol. 5, pp. 4738–4743.
[31] R. Pfiffner, "Optimal operation of CVT-based powertrains," Ph.D. dissertation, Swiss Federal Inst. Technol., Zurich, Swiss, 2001.
[32] M. André, "The ARTEMIS European driving cycles for measuring car pollutant emissions," *Sci. Total Environ.*, vol. 334/335, pp. 73–84, Dec. 2004.
[33] G. Vogelaar, "VT2+: Further improving the fuel economy of the VT2 transmission," in *Proc. 6th Int. Conf. Continuously Variable Hybrid Transm.*, Maastricht, The Netherlands, 2010, pp. 105–109.

Koos van Berkel (S'11) received the M.Sc. degree in mechanical engineering in 2007 from Eindhoven University of Technology, Eindhoven, The Netherlands, where he is currently working toward the Ph.D. degree with the Control Systems Technology Group in the field of control design for a mechanical hybrid powertrain.

His research interests are in the modeling and control of automotive powertrains and motion systems.

Theo Hofman received the Ph.D. degree in mechanical engineering from Eindhoven University of Technology, Eindhoven, The Netherlands, in 2007.

Since 2010, he has been an Assistant Professor with the Control Systems Technology Group, working in the field of vehicle propulsion systems. He is an Associate Editor of the *International Journal of Electric and Hybrid Vehicles*.

Dr. Hofman is an International Program Committee Member for the IEEE Vehicle, Propulsion, and Power Conference.

Bas Vroemen received the Ph.D. degree in the field of transmission component control of passenger cars with continually variable transmissions from Eindhoven University of Technology, Eindhoven, The Netherlands, in 2001.

He is currently a business partner within Drivetrain Innovations B.V. (DTI), which is a licensing and contract research center for automotive powertrains, transmissions, and components. He is an Editorial Board Member of the *International Journal of Powertrains*.

Maarten Steinbuch (S'83–M'89–SM'02) received the Ph.D. degree from Delft University of Technology, Delft, The Netherlands, in 1989.

Since 1999, he has been a Full Professor with the Control Systems Technology Group, Department of Mechanical Engineering, Eindhoven University of Technology, Eindhoven, The Netherlands. He is Editor-in-Chief of *IFAC Mechatronics* and Scientific Director of the Centre of Competence High Tech Systems of the Federation of Dutch Technical Universities. His research interests are in the modeling, design, and control of motion systems and automotive powertrains.